Tabriz Journal of Electrical Engineering (TJEE), vol. 55, no. 1, 2025 Serial no. 111
DOI: 10.22034/tjee.2024.61223.4830

Simplified High Resolution Template Simulator in SAR Seeker HWIL Simulation

Sima Shariatmadari, Seyed Mehdi Hosseini Andargoli*

Electrical and Computer Engineering Department, Noshirvani, Babol, Iran.
E-mail addresses: simashariatmadari@stu.nit.ac.ir, smh_andargoli@nit.ac.ir
*Corresponding author

Received 11/05/2024, Revised: 27/07/2024, Accepted:07/09/2024.

Abstract
With the development of high resolution synthetic aperture radar (SAR) technology, new challenges are emerging in the test stage of the SAR seekers using hardware in the loop (HWIL) simulation. In fact, in order to establish a confident HWIL simulation, the simulator should also generate the echo signal with the same resolution the SAR performs image processing. Echo signal generation by high resolution target template faces the issue of dealing with the incremental computation resources and contradicts with the real time requirement of HWIL simulation. In this paper, the potential of a very high resolution SAR test experiment by means of a lowered resolution simulator in HWIL simulation will be discussed. As the first step, we put forward a simple method of template resolution reduction to overcome the high time-consuming and computational resource requirement of high resolution SAR HWIL simulation and then theoretically explore the influence of template resolution reduction on the final SAR imaging. In this way, the resolution of the SAR seeker is kept fixed, and the scene simulator is forced to generate the echo signal at a lower resolution. In comparison to conventional echo signal generation, the proposed method can clearly better manage the hardware requirement of HWIL simulation and obtain acceptable imaging results. The results of the proposed method are compared with the reference one in terms of structural similarity index (SSIM) and the peak signal-to-noise ratio (PSNR) as performance evaluation criteria. Simulation results on an actual SAR template verify the good performance of the approach.
Keywords
High resolution synthetic aperture radar (SAR) imaging technology, hardware in the loop (HWIL) simulation, template resolution reduction.

1. Introduction

The final step in designing an operational radar is to analyse and evaluate it in a closed loop simulation process. This process is important in terms of error evaluation of the overall system [1]. The concept of hardware in the loop (HWIL) simulation is becoming one of the key aspects for developing, designing and testing stages of a wide variety of embedded systems, in which the mathematical model is replaced with the physical devices or subsystems. Simulations in the HWIL run at real-time, and are therefore substantially slower than of any less extensive approaches of software in the loop (SWIL). For the SWIL method, the code algorithms are embedded in a Simulink block. The blocks containing the code can be connected to the remaining blocks of the Simulink model. Thus, the software implementation of an algorithm can be easily verified and tested with simulated inputs. The objective in the SWIL is the verification of the source code of algorithms. In fact, the algorithms could be implemented in C++ code and the software modules are verified for correct implementation, but it will not consider the hardware issues. However, the hardware in the loop approach incorporates the actual hardware into the setup [2]. The most critical components in the hardware in the loop simulation are radar target simulators. They are used to emulate well-defined targets or scenarios to test radar sensors or the behaviour of entire systems that include such sensors [3]. Radar target simulators have been also widely applied in the test stage of automotive radar sensors in autonomous driving.

[4] provides with a modular design of a multi angle multi target radar target simulator integrated into an existing and adapted steerable vehicle in the loop test bench which forms an advanced validation setup for advanced driver assistance system functions that incorporates radar sensing. [5] proposes a novel approach for the generation of targets with flexible direction of arrival in automotive radar target simulator applications. This concept is established by using coherently modulated target elements placed around the radar sensor under test which enables a joint direction of arrival simulation. [6] investigates the generation of targets for frequency modulated continuous wave chirp sequence radar in the close range of vehicles surrounding. The proposed radar target simulator has no delay lines to simulate the range, instead it is modulated directly. The simulation in range is realized by directly shifting the radar signal to the corresponding beat frequency. In [7] a general model and simulation scheme for the concept of coherent direction of arrival simulation with arbitrary radar array configurations is derived. The proposed model in this study allows the calculation of the required target simulator's amplitudes and phases or time delays without constraints concerning the number of radar channels, array geometries or employed beam-formers when the channel is known priory. [8] presents a system capable of

generating multiple targets with individual ranges and velocities for chirp-sequence frequency modulated continuous waveform radars without prior knowledge about the radar sensor by estimating the radar's waveform parameters. Due to the high resolution of recent radar sensors in both range and cross range directions, [9] proposes a method to synthesize the range Doppler migration phenomenon in radar target simulation. The concept of synthetic aperture radar (SAR) scene simulation has also been investigated in [10-12]. They all provide with an efficient Fourier domain SAR raw signal simulator which is able to deal with extended scene in case of an ideal straight-line sensor flight path. However, to the best of our knowledge it has not been yet surveyed in terms of hardware resource consumption. In fact, the main idea in this study is to reduce the hardware consumption in HWIL simulation when dealing with a high resolution SAR system.

Imaging radars are the radars with high resolution accuracy that have been heavily used due to applications in target identification, imaging in different atmospheric conditions and etc. The idea of these radars developed due to the low azimuthal resolution of traditional radars [13]. Conventional SAR data offer spatial resolution of the order of tens to hundreds of meters [14]. The resolution issue for missile-borne SAR seekers is not so problematic. This is because the missile borne SAR seeker is considered in the context of positioning and targeting sea/land targets as opposed to high resolution imaging [15]. However, present day high resolution SAR sensors can achieve up to 1-meter spatial resolution and sub meter resolution will be realized in future SAR missions [14,16]. When using a high sample rate, the storage ability of the digital radio frequency memory (DRFM) system should greatly be extended and computing resource (run-time and memory usage) requirements will be increased drastically, which will impose a great challenge for digital signal processing (DSP) or field-programmable gate array (FPGA) real time processes [17]. In this study, in order to fulfil the real time requirement and computation resource limitation along with preserving the quality of imaging results in HWIL simulation of high resolution SAR seekers, we propose spatial and temporal resolution reduction and explore its feasibility using simulation environment. The template resolution reduction could be conducted by roughly advancing time in small, discrete steps to preserve a predefined degree of accuracy. The amount in which this reduction rate is used can be heuristically varied, resulting in a trade-off between quality of the final image and computational complexity.

Although the application of HWIL simulation for SAR seeker evaluation is well studied in [18,19], the concept of reduced resolution of the target template was not studied yet. A block diagram of the proposed method is shown in Fig. 1(b) along with the conventional method of Fig. 1(a).

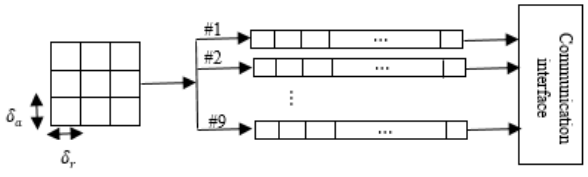

(a)

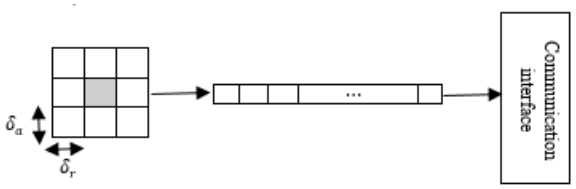

(b)

Fig. 1. Block Diagram of (a) the Conventional Method (b) the Proposed One.

Where δ_r and δ_a indicate the resolution along the range and azimuth directions, respectively. As shown in Fig. 1(b) according to a predefined reduction rate, a reduced number of cells will be stored in the buffer to be uploaded on the communication interface.

In fact, a number of distinct range and cross range resolution reductions along with combined reduction schemes are simulated and applied to the high resolution target template. The quality of imaging results is evaluated by comparing with a non-reduced reference case. As is apparent, the improvement in reducing the computational resource utilization will be obtained at the cost of image quality reduction. A detailed description of the proposed method will be explained in the following sections.

The paper is organized as follows. Section 2 reviews the existing technique for full resolution target template echo signal generation in SAR seeker HWIL simulation. The proposed alternative reduced resolution method is presented in section 3, followed by the error influence analysis discussion. Finally, the simulation based evaluation results along with the final conclusions are provided in section 4 and 5, respectively.

2. Overview on Conventional Echo Signal Generation Model

The overall block diagram of the SAR HWIL simulation is shown in Fig. 2. In this scheme, the master control unit initiates/terminates the HWIL simulation, it also provides the flight trajectory based details according to the specified information updating rate. The scene modulation signal computation for an extended SAR scene is performed on parallel FPGAs in the scene processing unit. The wideband DREM gathers the whole scene modulation signal and the digitized down-converted SAR raw signal to perform the fast convolution in the frequency domain and outputs the generated echo signal to the SAR antenna after digital to analogue and up-conversion.

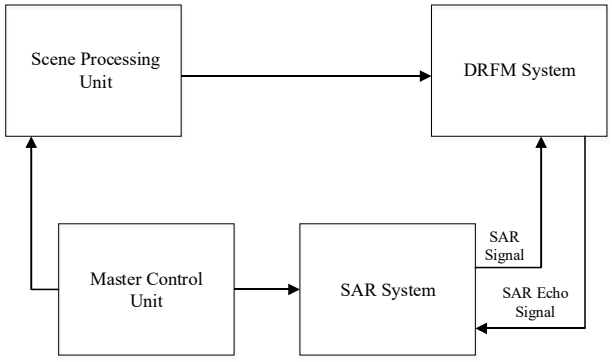

Fig. 2. Overall SAR HWIL System Diagram.

Generally, the transmitted signal in SAR application is a linear frequency modulated (LFM) signal having a bandwidth B centred around the carrier frequency f_0 defined as:

$$S_t(t) = a(t)exp\big(j(2\pi f_0 t + \pi k_r t^2 + \varphi)\big) \quad (1)$$

Where $a(t)$ is a rectangular pulse, K_r is the chirp rate, and φ is the constant initial phase which is neglected in the proceeding analysis.

The received SAR raw data from (m,n)th scattering point is well presented in [20,21] as (2);

After down-conversion we do have (3);

With $SMS^{mn}(t,\eta) = \sigma_{mn}e^{-j\frac{4\pi}{\lambda}R_{mn}(\eta)}\delta(t-\tau_{mn}(\eta))$ and $S(t) = a(t)e^{j\pi k_r t^2}$ as the scene modulation signal and the baseband LFM signal transmitted by the seeker, respectively.

In the nominal condition we sample these two predefined functions as shown in (4) and (5); and then convolve them to generate the echo signal.

$$SMS^{mn}[i,l] = \sigma_{mn}e^{-j\frac{4\pi}{\lambda}R_{mn}[l]}\delta\big[i-\tau_{mn}[l]\big] \quad (4)$$

$$S[i] = a[i]e^{j\pi k_r i^2} \quad (5)$$

By convolving the scene modulation signal with the received LFM signal, we do have (6) for the generated echo signal,

Where $*_i$ indicates convolution along the range direction. This echo signal will be gathered by the seeker and goes through the SAR image formation procedure of (7) to produce the final imaging result.

$$I^{mn}(i,l) = S_r[i,l] * MF_r[i] * MF_a[l] \quad (7)$$

Where $MF_r[i]$ and $MF_a[l]$ defined in (8) and (9) correspond to the match filter definition along the range and azimuth direction, respectively.

$$MF_r[i] = a[i]e^{-j\pi k_r i^2} \quad (8)$$

$$MF_a[l] = b[l]e^{-j\pi k_a l^2} \quad (9)$$

In the above definition $b[l]$ is a rectangular function defined in synthetic aperture time interval of T_s and $k_a = \frac{-2v^2}{(X_c+x_m)\lambda}$ is the azimuth chirp rate; If we could approximate the instant slant range equation as (10);

Then the echo signal could be rewritten as (11);

After match filter processing along the range direction, we do expect (12) as the match filter output;

By neglecting the constant and the coupling terms between the range and azimuth dimensions, the SAR two dimensional image would be obtained after azimuth match filtering, as (13):

While the final approximation of the compressed output will be valid for sufficiently large time-bandwidth products for both range and azimuth signals. As the final step we sum up to obtain the whole extended scene image;

$$I(i,l) = \sum_n \sum_m I^{mn}(i,l) \quad (14)$$

This method is high memory demanded and not suitable for high resolution SAR seekers. The increase in template resolution lead to a rapid increase of computation effort for echo signal generation. So the time required to generate a high resolution echo component will increase dramatically when external memory is conducted as a sole possible solution. Following we investigate an alternative echo signal generation to reduce the computing resources required to solve the problem without significant reduction of final image quality.

3. Principle of the Proposed Method

We define the impulse functions $p(t)$ and $q(\eta)$ as the sampling functions of the scene modulation signal with the sampling frequencies f_{s1} and f_{s2}, respectively.

$$p(t) = \sum_{i=-\infty}^{+\infty}\delta(t-\frac{i}{f_{s1}}) \quad (15)$$

$$q(\eta) = \sum_{l=-\infty}^{+\infty}\delta(\eta-\frac{l}{f_{s2}}) \quad (16)$$

As a result of this change in the echo signal model, we could obtain the new sampled expression of the original SAR scene modulation signal as (17),

$$S_r(t,\eta) = \sigma_{mn}a(t-\tau_{mn}(\eta))e^{j2\pi f_0(t-\tau_{mn}(\eta))+j\pi k_r(t-\tau_{mn}(\eta))^2} \quad (2)$$

$$S_r(t,\eta) = \sigma_{mn}a(t-\tau_{mn}(\eta))e^{-j\frac{4\pi}{\lambda}R_{mn}(\eta)+j\pi k_r(t-\tau_{mn}(\eta))^2} = SMS^{mn}(t,\eta) * S(t) \quad (3)$$

$$S_r[i,l] = SMS^{mn}[i,l] * S[i] = \sigma_{mn}e^{-j\frac{4\pi}{\lambda}R_{mn}[l]}\delta\big[i-\tau_{mn}[l]\big] *_i a[i]e^{j\pi k_r i^2} = \sigma_{mn}e^{-j\frac{4\pi}{\lambda}R_{mn}[l]}a\big[i-\tau_{mn}[l]\big]e^{j\pi k_r[i-\tau_{mn}[l]]^2} \quad (6)$$

$$R_{mn}[l] = \sqrt{(X_c+x_m)^2+(vl+y_n)^2} \approx (X_c+x_m)+\frac{(vl+y_n)^2}{2(X_c+x_m)} = (X_c+x_m)+\frac{\left(l+\frac{y_n}{v}\right)^2}{\frac{2(X_c+x_m)}{v^2}} \quad (10)$$

$$S_r[i,l] = \sigma_{mn}e^{-j\frac{4\pi}{\lambda}\left[(X_c+x_m)+\frac{\left(l+\frac{y_n}{v}\right)^2}{\frac{2(X_c+x_m)}{v^2}}\right]}a\big[i-\tau_{mn}[l]\big]e^{j\pi k_r[i-\tau_{mn}[l]]^2} \quad (11)$$

$$S_r[i,l] * MF_r[i] = \sigma_{mn}e^{-j\frac{4\pi}{\lambda}\left[(X_c+x_m)+\frac{\left(l+\frac{y_n}{v}\right)^2}{\frac{2(X_c+x_m)}{v^2}}\right]}a\big[i-\tau_{mn}[l]\big]e^{j\pi k_r[i-\tau_{mn}[l]]^2} * a[i]e^{-j\pi k_r i^2} = \sigma_{mn}e^{-j\frac{4\pi}{\lambda}\left[(X_c+x_m)+\frac{\left(l+\frac{y_n}{v}\right)^2}{\frac{2(X_c+x_m)}{v^2}}\right]}\big(T_p-|i-\tau_{mn}[l]|\big)sinc\big[k_r(i-\tau_{mn}[l])\big(T_p-|i-\tau_{mn}[l]|\big)\big] \quad (12)$$

$$I^{mn}(i,l) = \sigma_{mn}e^{j\pi k_a\left(l+\frac{y_n}{v}\right)^2}\left(T_p f_r-\left|i-\frac{2(X_c+x_m)}{c}f_r\right|\right)sinc\left[k_r\left(i-\frac{2(X_c+x_m)}{c}f_r\right)\left(T_p f_r-\left|i-\frac{2(X_c+x_m)}{c}f_r\right|\right)\right] * b[l]e^{-j\pi k_a l^2} = \sigma_{mn}\left(T_p f_r-\left|i-\frac{2(X_c+x_m)}{c}f_r\right|\right)\left(T_s f_a-\left|l+\frac{y_n}{v}f_a\right|\right)sinc\left[k_r\left(i-\frac{2(X_c+x_m)}{c}f_r\right)\left(T_p f_r-\frac{2(X_c+x_m)}{c}f_r\right)\right]sinc\left[k_a\left(l+\frac{y_n}{v}f_a\right)\left(T_s f_a-\left|l+\frac{y_n}{v}f_a\right|\right)\right] \approx \sigma_{mn}T_pT_s sinc\left[k_rT_p\left(i-\frac{2(X_c+x_m)}{c}f_r\right)\right]sinc\left[k_aT_s\left(l+\frac{y_n}{v}f_a\right)\right] \quad (13)$$

$$SMS^{mn}(t,\eta) = \sigma_{mn}e^{-j\frac{4\pi}{\lambda}R_{mn}(\eta)}\delta\big(t-\tau_{mn}(\eta)\big)\times\sum_{i=-\infty}^{+\infty}\delta\left(t-\frac{i}{f_{s1}}\right)\times\sum_{l=-\infty}^{+\infty}\delta(\eta-\frac{l}{f_{s2}}) \quad (17)$$

We should also conduct a sampling procedure for the pure LFM signal to perform the convolution in the time domain. The rest of the image processing will be accomplished on received echo signal after up sampling.

Knowing the fact that the new sampling frequencies are integer fractions of SAR sampling frequencies as $f_{s1} = \left\lfloor \frac{f_r}{h} \right\rfloor$ and $f_{s2} = \left\lfloor \frac{f_a}{g} \right\rfloor$, with f_r and f_a as the range and azimuth sampling frequencies and $h, g > 1$, we could write the corresponding range and azimuth displacement error of each scattering point induced by this rough approximation as follows:

$$0 < \varepsilon_r^{mn} < h - 1 \quad (18)$$

$$0 < \varepsilon_a^{mn} < g - 1 \quad (19)$$

According to the predefined reduced resolution method, we have (20) for the I^{mn}, with the certain peak deviations from the original location.

Determining the average error of the final imaging result is the key issue of the proposed method, so detailed error analysis is the focus of our proceeding mathematical discussion.

If we suppose the uniform distribution for both error terms, that is,

$$\varepsilon_r^{mn} \sim U[0, h-1] \quad (21)$$

$$\varepsilon_a^{mn} \sim U[0, g-1] \quad (22)$$

And knowing the fact that the two induced errors will have independent distribution, we could conduct an expression for the average error of the proposed method as (23).

The average imaging error induced by the template resolution reduction as a function of displacement error is sketched in Fig. 3.

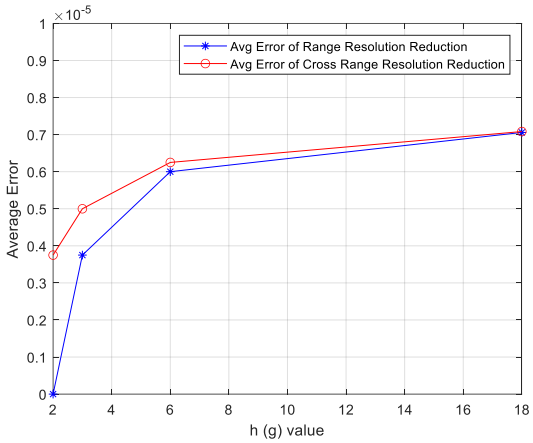

Fig. 3. Average Error of the Proposed Method in Range and Cross Range Directions.

4. Simulation Results

This section provides a number of simulation experiments on performance comparison of SAR imaging results with the convention and novel target template sampling procedure. Simulation parameters are listed in Table I.

Table I. Simulation Parameters.

Parameter	Symbol	Value
Pulse Repetition Frequency	PRF	2000 Hz
Carrier Frequency	f_0	10 GHz
Velocity of the Platform	V	2000 m/s
Pulse Duration	T_p	25 μs
Instantaneous Bandwidth	B	150 MHz
Slant Range to the Centre of the Area	R_0	30 Km
Synthetic Aperture Time	T_s	0.3s

To verify the feasibility of the proposed resolution reduction method, an actual SAR template of Fig. 4.a is tested. First, a reference template without any reduction was carried out and followed by several reduced resolution ones and compared with the reference one. The sampling rate was reduced to 50%, 33.33%, 16.67%, 6.66% and 50%, 33.33%, 16.67%, 5.55% of the original target template in range and cross range, respectively. The difference between the two images indicates the effect of the resolution reduction process.

(a)

$$I_{new}^{mn}(i,l) = \sigma_{mn} T_p T_s sinc\left[k_r T_p \left(i - \frac{2(X_c + x_m)}{c} f_r + \varepsilon_r^{mn}\right)\right] sinc\left[k_a T_s \left(l + \frac{y_n}{v} f_a + \varepsilon_a^{mn}\right)\right] \quad (20)$$

$$E\{I_{new}^{mn}(i,l) - I^{mn}(i,l)\} = E\left\{\sigma_{mn} T_p T_s sinc\left[k_r T_p \left(i - \frac{2(X_c + x_m)}{c} f_r + \varepsilon_r^{mn}\right)\right] sinc\left[k_a T_s \left(l + \frac{y_n}{v} f_a + \varepsilon_a^{mn}\right)\right] - \sigma_{mn} T_p T_s sinc\left[k_r T_p \left(i - \frac{2(X_c + x_m)}{c} f_r\right)\right] sinc\left[k_a T_s \left(l + \frac{y_n}{v} f_a\right)\right]\right\} = \sigma_{mn} T_p T_s E\left\{sinc\left[k_r T_p \left(i - \frac{2(X_c + x_m)}{c} f_r + \varepsilon_r^{mn}\right)\right]\right\} E\left\{sinc\left[k_a T_s \left(l + \frac{y_n}{v} f_a + \varepsilon_a^{mn}\right)\right]\right\} - \sigma_{mn} T_p T_s sinc\left[k_r T_p \left(i - \frac{2(X_c + x_m)}{c} f_r\right)\right] sinc\left[k_a T_s \left(l + \frac{y_n}{v} f_a\right)\right] = \sigma_{mn} T_p T_s \frac{1}{(h-1)(g-1)} \sum_{\varepsilon_r^{mn}=0}^{h-1} sinc\left[k_r T_p \left(i - \frac{2(X_c + x_m)}{c} f_r + \varepsilon_r^{mn}\right)\right] \sum_{\varepsilon_a^{mn}=0}^{g-1} sinc\left[k_a T_s \left(l + \frac{y_n}{v} f_a + \varepsilon_a^{mn}\right)\right] - \sigma_{mn} T_p T_s sinc\left[k_r T_p \left(i - \frac{2(X_c + x_m)}{c} f_r\right)\right] sinc\left[k_a T_s \left(l + \frac{y_n}{v} f_a\right)\right] \quad (23)$$

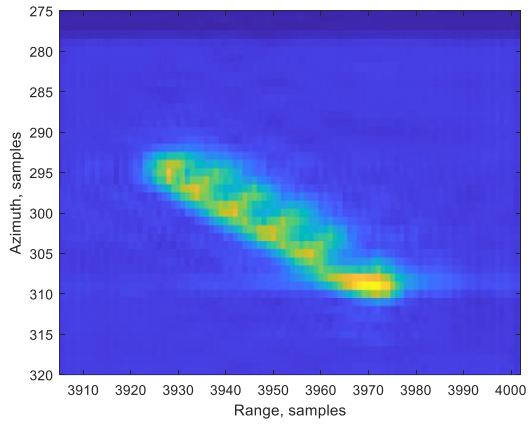

(b)

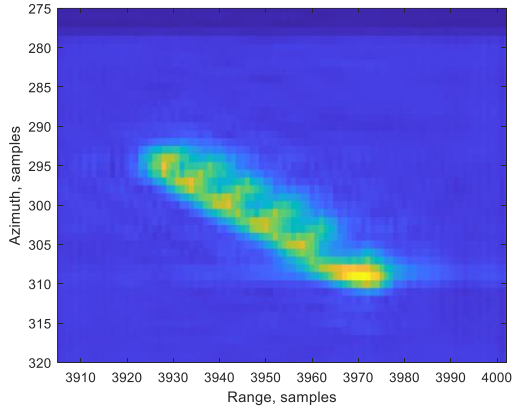

(c)

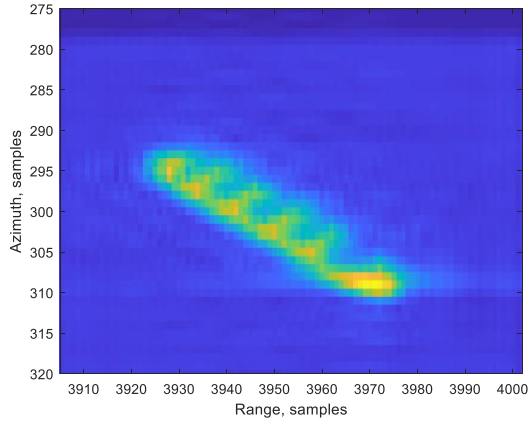

(d)

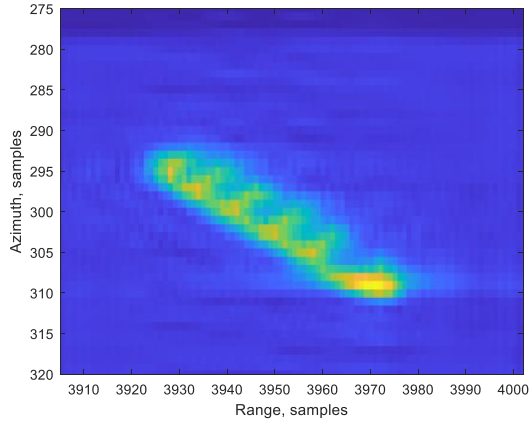

(e)

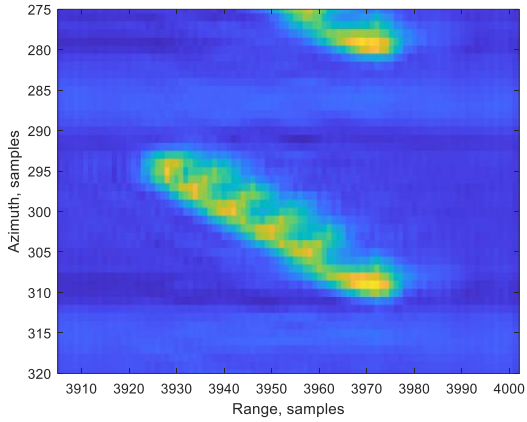

(f)

Fig. 4. Imaging Result of an actual SAR template. (a) Target Template, (b) Conventional Method, (c) Sampling Rate of (50%,50%), (d) Sampling Rate of (33.33%,33.33%), (e) Sampling Rate of (16.67%,16.67), (f) Sampling Rate of (6.66%,5.55%).

Two evaluation metrics are used to explore the similarity between the obtained image of the state of the art echo signal generation method and our proposed alternative one, which are peak signal to noise ratio (PSNR) and structural similarity index measurement (SSIM). The SSIM similarity index as a final visual quality metric provides a value between 0 and 1, with 1 and 0 indicating the highest and lowest level of similarity, respectively.

Consider x and y as the two desired images, then the SSIM metric is defined by the following relation [22,23]:

$$SSIM(x,y)=[l(x,y)]^{\alpha}[c(x,y)]^{\beta}[s(x,y)]^{\gamma} \quad (24)$$

With the terms $l(x,y)$, $c(x,y)$ and $s(x,y)$ as the comparison of luminance, contrast and structural correlation of the signals, respectively which are defined as follows,

$$l(x,y)=\frac{2\mu_x\mu_y+C_1}{\mu_x^2+\mu_y^2+C_1} \quad (25)$$

$$c(x,y)=\frac{2\sigma_x\sigma_y+C_2}{\sigma_x^2+\sigma_y^2+C_2} \quad (26)$$

$$s(x,y)=\frac{\sigma_{xy}+C_3}{\sigma_x\sigma_y+C_3} \quad (27)$$

In the above equations, the parameters α, β and γ determine the relative importance of each component, μ_x and μ_y are the means of two x and y input image blocks, respectively, σ_x and σ_y are the standard deviations, σ_x^2 and σ_y^2 denote the variances, respectively. σ_{xy} is the covariance of the two images. C_1, C_2 and C_3 are regularizing factors introduced for dealing with small amount of denominator.

With the same notation, the PSNR value for an n-bit grayscale image will be defined by the following expression [24];

$$PSNR(x,y)=10\,log_{10}\left(\frac{(2^n-1)^2}{MSE(x,y)}\right) \quad (28)$$

While the numerator is the highest dynamic range achievable by the image function [22] and in the case of a grey scale image of 8 bits is equal to 255 [25]; the denominator of the PSNR is the MSE defined as follows [24];

$$MSE(x,y)=\frac{1}{MN}\sum_{i=1}^{M}\sum_{j=1}^{N}\left(x_{ij}-y_{ij}\right)^2 \quad (29)$$

The PSNR value approaches infinity as the MSE approaches zero; this shows that a higher PSNR value provides a higher image quality. At the other end of the scale, a small value of the PSNR implies high numerical differences between images [26]. The SSIM and PSNR indices by different methods are depicted in Table II.

Table II. Imaging Evaluation Using SSIM and PSNR Metrics.

	SSIM	PSNR
(0.5,0.5)	0.9998	46.1216
(0.3333,0.3333)	0.9995	42.4363
(0.1667,0.1667)	0.9989	38.6717
(0.0555,0.0666)	0.9745	22.7342

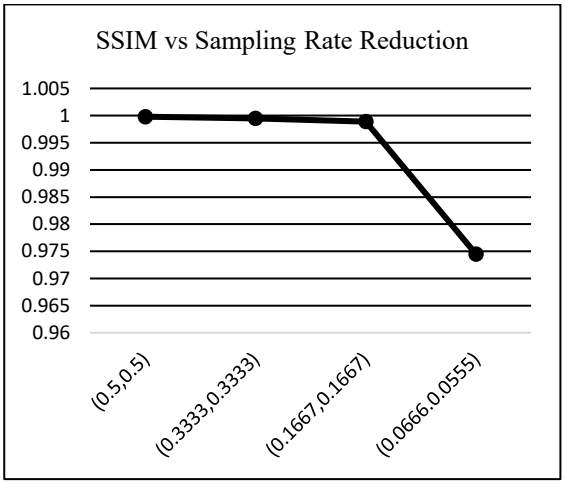

(a)

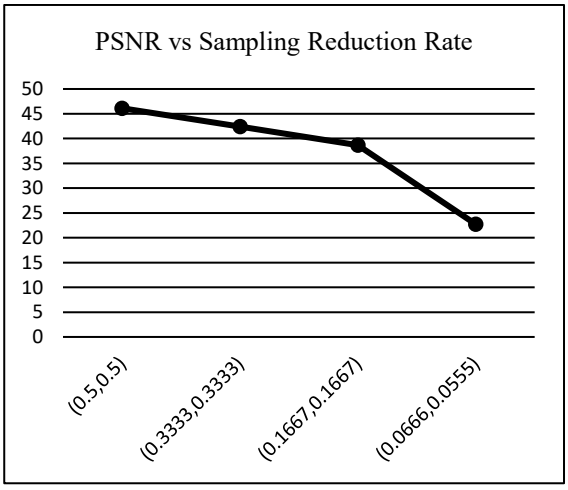

(b)

Fig. 5. Schematic Comparison of Imaging Results graph. (a) SSIM vs Sampling Rate Reduction, (b) PSNR vs Sampling Reduction Rate.

The PSNR and SSIM results are relatively good when the sampling reduction rate will not exceed 83.33% in both range and cross range dimensions. In fact, the results of 6.66% and 5.55% sampling rate hardly converge to the reference image. Consequently, as is depicted in Fig. 1(b), depending on the selected reduction rate, the number of utilized buffers will be reduced accordingly with an acceptable image quality.

In all simulation procedures, the contribution of thermal noise is not considered at all. Fig. 5 shows the impact of the applied approach on the final imaging results in terms of these two different metrics.

We suspect that the resolution reduction approach in range and cross range directions may affect the imaging result differently. Following, to find out which dimension more seriously deteriorates the imaging quality, we break up the reduction procedure and put forward their individual effect by keeping the reciprocal reduction rate fixed. The simulation results corresponding to detached reductions are provided in Fig. 6 and 7.

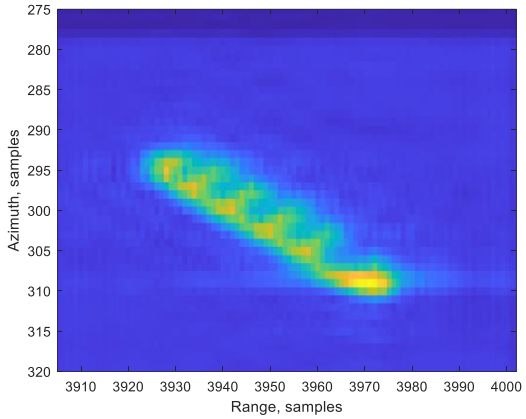

(a)

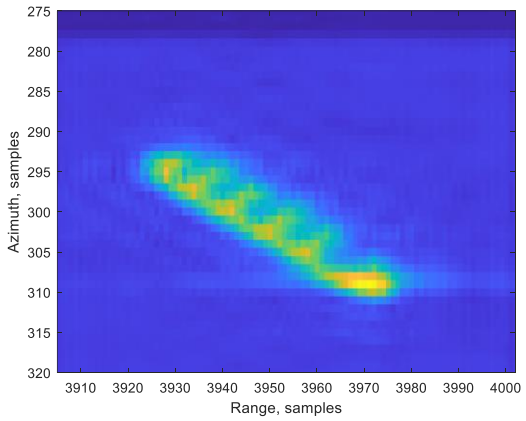

(b)

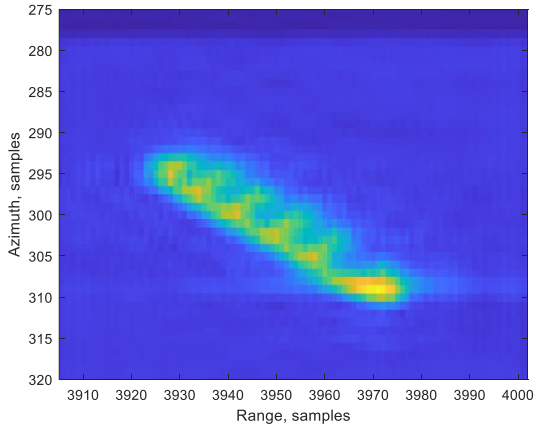

(c)

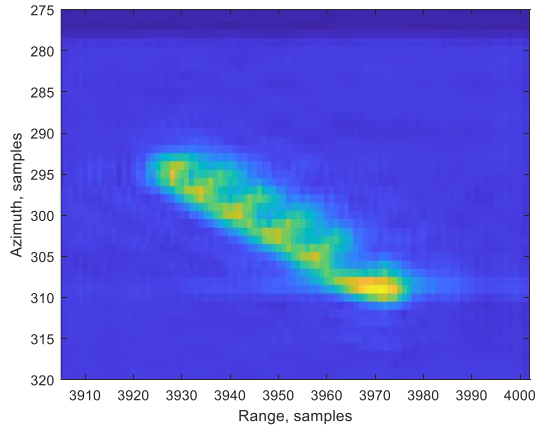

(d)

Fig. 6. Imaging Results Using Range Resolution Reduction. (a) Sampling Rate of 50%, (b) Sampling Rate of 33.33%, (c) Sampling Rate of 16.67%, (d) Sampling Rate of 5.55%.

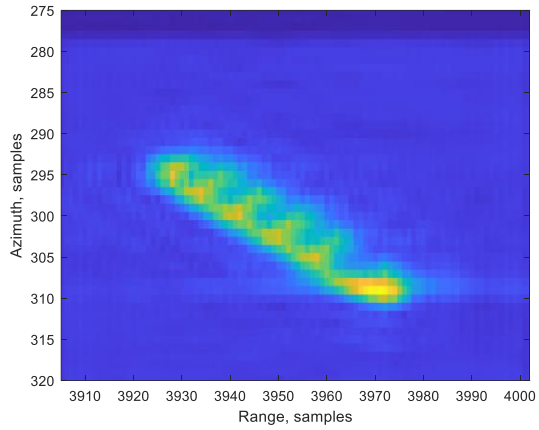

(a)

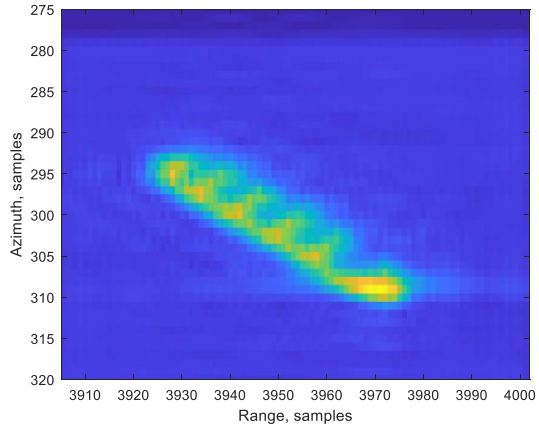

(b)

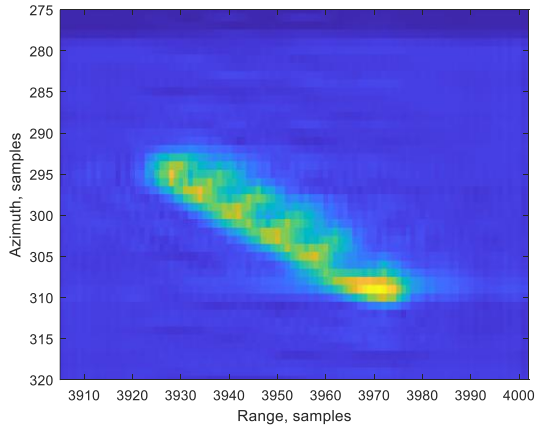

(c)

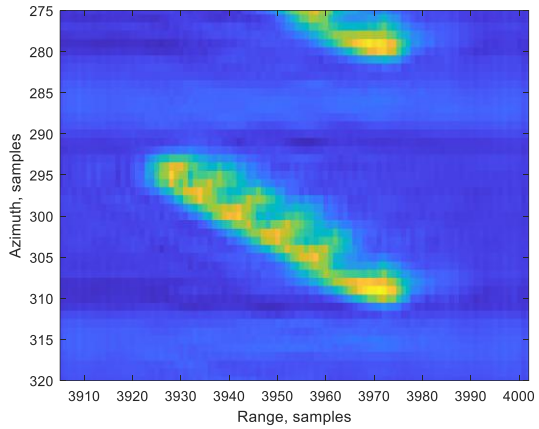

(d)

Fig. 7. Imaging Results Using Cross Range Resolution Reduction. (a) Sampling Rate of 50%, (b) Sampling Rate of 33.33%, (c) Sampling Rate of 16.67%, (d) Sampling Rate of 6.66%.

Although the outcomes attained by range resolution reduction, visually demonstrate a more acceptable performance, in order to establish a fair comparison, the imaging results are evaluated using the previously defined metrics depicted in Fig. 8 and Fig.9.

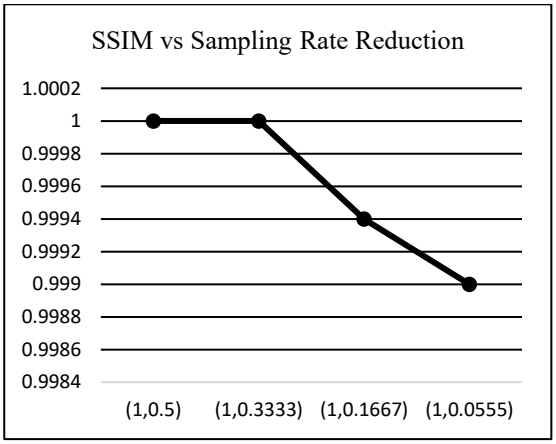

(a)

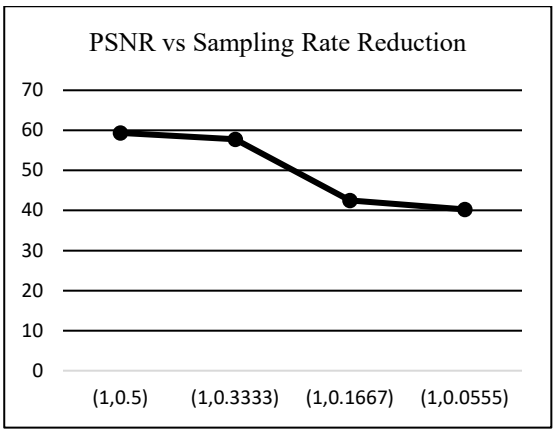

(b)

Fig. 8. Schematic Comparison of Imaging Metrics by Range Resolution Reduction. (a) SSIM vs Sampling Rate Reduction, (b) PSNR vs Sampling Rate Reduction.

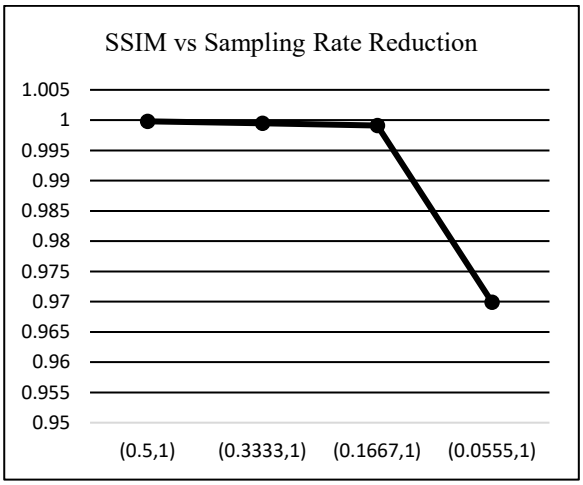

(a)

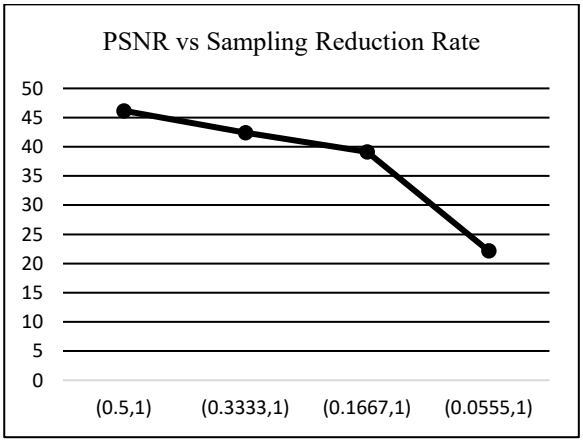

(b)

Fig. 9. Schematic Comparison of Imaging Metrics by Cross Range Resolution Reduction. (a) SSIM vs Sampling Rate Reduction, (b) PSNR vs Sampling Reduction Rate.

Besides, all comparisons are also shown in tabular form in Table III and Table IV.

Table III. Imaging Evaluation Using SSIM and PSNR Metrics by Range Resolution Reduction.

	SSIM	PSNR
(1,0.5)	1	57.7699
(1,0.3333)	1	59.3613
(1,0.1667)	0.9994	42.4935
(1,0.0555)	0.9990	40.2643

Table IV. Imaging Evaluation Using SSIM and PSNR Metrics by Cross Range Resolution Reduction.

	SSIM	PSNR
(0.5,1)	0.9998	46.1684
(0.3333,1)	0.9995	42.4243
(0.1667,1)	0.9991	39.1205
(0.0666,1)	0.9699	22.1574

We conclude that fewer deviations from the reference image will appear when applying range resolution reduction and imaging quality more severely deviates from the reference target template as the cross range reduction rate increases. Because this one, we recommend avoiding the cross range resolution reduction if range resolution reduction will satisfy the computational resource requirement.

The previously theoretical assumed problems with resolution reduction in both range and cross range direction are thus confirmed and the presented imaging results of the proposed method based on high resolution SAR seeker verifies the potential of HWIL utilization in forthcoming high resolution SAR seekers.

5. Conclusion

Future space-borne SAR systems will be required to produce high resolution images in both range and cross range dimensions. However, the computational resource and real time constraint of the conventional SAR HWIL simulations make it difficult to increase the resolution of the simulator in the test stage. This paper investigates the influence of lower target template resolution in echo signal generation procedure. The approach first applies two sampling functions to the scene modulation signal and proceeds the mathematical analysis in discrete time domain, then introduces the displacement error induced by this reduction rate. An average error expression is also obtained to facilitate the final imaging evaluation. The simulation results could be utilized as a guideline for application based target template resolution selection.

6. References

[1] ENTEZARI, R.; RASHIDI, A. J. Inverse Synthetic Aperture Radar (ISAR) Imaging of Targets with Non-Uniform Motion. TABRIZ JOURNAL OF ELECTRICAL ENGINEERING, 2017, 47.2: 391-400 (in Persian).

[2] KIESBYE, Jonis, et al. Hardware-in-the-loop and software-in-the-loop testing of the move-ii cubesat. *Aerospace*, 2019, 6.12: 130.

[3] BIRKENHAUER, Christoph, et al. A simple and versatile concept to improve dynamic range and enable target angle adaptability in radar target simulators. *IEEE Journal of Microwaves*, 2023.
[4] DIEWALD, Axel, et al. Radar target simulation for vehicle-in-the-loop testing. *Vehicles*, 2021, 3.2: 257-271.
[5] SCHOEDER, Pirmin, et al. Flexible direction-of-arrival simulation for automotive radar target simulators. *IEEE Journal of Microwaves*, 2021, 1.4: 930-940.
[6] IBERLE, Johannes; RIPPL, Patrick; WALTER, Thomas. A near-range radar target simulator for automotive radar generating targets of vulnerable road users. *IEEE Microwave and Wireless Components Letters*, 2020, 30.12: 1213-1216.
[7] SCHOEDER, Pirmin, et al. A unified model of coherent direction-of-arrival simulation for radar target simulators. *IEEE Transactions on Aerospace and Electronic Systems*, 2023, 59.4: 4738-4743.
[8] SCHOEDER, Pirmin, et al. Multitarget simulator for automotive radar sensors with unknown chirp-sequence modulation. *IEEE Microwave and Wireless Components Letters*, 2021, 31.9: 1086-1089.
[9] DIEWALD, Axel, et al. Range Doppler migration synthesis for realistic radar target simulation. In: *2021 IEEE Topical Conference on Wireless Sensors and Sensor Networks (WiSNeT)*. IEEE, 2021. p. 56-58.
[10] FRANCESCHETTI, Giorgio, et al. SARAS: A synthetic aperture radar (SAR) raw signal simulator. *IEEE Transactions on Geoscience and Remote Sensing*, 1992, 30.1: 110-123.
[11] FRANCESCHETTI, Giorgio; MIGLIACCIO, Maurizio; RICCIO, Daniele. SAR raw signal simulation of actual ground sites described in terms of sparse input data. *IEEE Transactions on Geoscience and Remote Sensing*, 1994, 32.6: 1160-1169.
[12] FRANCESCHETTI, Giorgio, et al. SARAS: A synthetic aperture radar (SAR) raw signal simulator. *IEEE Transactions on Geoscience and Remote Sensing*, 1992, 30.1: 110-123.
[13] TOREINIA, R.; KAZEROONI, M.; FALLAH, M. Analysis and Evaluation of Important Antenna and Radome Parameters Effect on the Angle Measurement of a Monopulse Radar Simulator for a Projectile Platform. *TABRIZ JOURNAL OF ELECTRICAL ENGINEERING*, 2018, 47.4: 1381-1393 (in Persian).
[14] KIM, Duk-jin, et al. Melt pond mapping with high-resolution SAR: The first view. *Proceedings of the IEEE*, 2013, 101.3: 748-758.
[15] SAEEDI, Jamal. Feasibility study and conceptual design of missile-borne synthetic aperture radar. *IEEE Transactions on Systems, Man, and Cybernetics: Systems*, 2017, 50.3: 1122-1133.
[16] REALE, Diego, et al. Tomographic imaging and monitoring of buildings with very high resolution SAR data. *IEEE Geoscience and remote sensing letters*, 2011, 8.4: 661-665.
[17] ZONGBO, Wang, et al. Design and application of DRFM system based on digital channelized receiver. In: 2008 International Conference on Radar. IEEE, 2008. p. 375-378.
[18] SHU, Ting, et al. Development of multichannel real-time Hardware-in-the-Loop radar environment simulator for missile-borne Synthetic Aperture Radar. In: 2015 IEEE Radar Conference (RadarCon). IEEE, 2015. p. 0368-0373.
[19] HE, Zhihua, et al. A hardware-in-loop simulation and evaluation approach for spaceborne distributed SAR. In: 2011 IEEE International Geoscience and Remote Sensing Symposium. IEEE, 2011. p. 886-889.
[20] ZHANG, Shunsheng; CHEN, Juan. A echo simulation algorithm for natural scene. In: *2008 International Conference on Radar*. IEEE, 2008. p. 464-468.
[21] SHU, Ting, et al. Development of multichannel real-time Hardware-in-the-Loop radar environment simulator for missile-borne Synthetic Aperture Radar. In: *2015 IEEE Radar Conference (RadarCon)*. IEEE, 2015. p. 0368-0373.
[22] BRUNET, Dominique; VRSCAY, Edward R.; WANG, Zhou. On the mathematical properties of the structural similarity index. *IEEE Transactions on Image Processing*, 2011, 21.4: 1488-1499.
[23] ZUJOVIC, Jana; PAPPAS, Thrasyvoulos N.; NEUHOFF, David L. Structural texture similarity metrics for image analysis and retrieval. *IEEE Transactions on Image Processing*, 2013, 22.7: 2545-2558.
[24] C. W. Kok and W. S. Tam, “Image Quality,” in Digital Image Interpolation in Matlab, John Wiley & Sons, 2019, ch. 3, pp. 71–90.
[25] FARDO, Fernando A., et al. A formal evaluation of PSNR as quality measurement parameter for image segmentation algorithms. *arXiv preprint arXiv:1605.07116*, 2016.
[26] HORE, Alain; ZIOU, Djemel. Image quality metrics: PSNR vs. SSIM. In: 2010 20th international conference on pattern recognition. IEEE, 2010. p. 2366-2369.